American Journal of Transplantation
Wiley Periodicals Inc.

doi: 10.1111/ajt.12148

Reciprocal Interaction Between Intestinal Microbiota and Mucosal Lymphocyte in Cynomolgus Monkeys After Alemtuzumab Treatment

Q. R. Li, C. Y. Wang, C. Tang, Q. He, N. Li and J. S. Li*

Research Institute of General Surgery, Jinling Hospital, Nanjing University School of Medicine, Nanjing, China
** Corresponding author: Q. R. Li or J. S. Li*
liqiurong@yahoo.com or lijieshounju@163.com

It has been known that the gut microbiota plays a central role in shaping normal mucosal immunity, however, little information is available whether the variability of mucosal lymphocytes impacts the commensal flora. Here, we applied a cynomolgus monkey model to characterize the structure and composition of the gut microbiota in response to lymphocyte depletion and to determine their potential association. Molecular profiling of 16S rDNA showed that the intestinal microbiota composition was perturbed after the depletion of mucosal lymphocytes and were recovered following the repopulation. Some specific bacteria from the orders Lactobacillales, Enterobacteriales and Clostridiales, and the genus Prevotella and Faecalibacterium, were primarily responsible for the variations of the gut microbiota after lymphocyte depletion. Interestingly, the species richness of the ileal mucosal microbiota was associated the proportions of TCR$\alpha\beta^+$ or TCR$\gamma\delta^+$ T cells ($p < 0.01$). We demonstrate for the first time the feature of intestinal microbiota composition after lymphocyte depletion and provide novel evidence that the perturbation of gut microbiota is associated with lymphocyte depletion. It may contribute to understand the relationship between gut commensal microbiota and mucosal immune system. Study results provide insight into biological activity of alemtuzumab in intestinal barrier in organ transplantation.

Key words: Alemtuzumab, denaturing gradient gel electrophoresis, DNA sequencing, intestinal microbiota, lymphocyte depletion

Abbreviations: DGGE, denaturing gradient gel electrophoresis; IEL, intestinal intraepithelial lymphocyte; LPL, lamina propria lymphocyte.

Received 05 July 2012, revised 20 November 2012 and accepted for publication 17 December 2012

Introduction

Alemtuzumab (Campath-1H) is a humanized anti-CD52 monoclonal antibody and it targets CD52 expressed on T and B lymphocytes, natural killer (NK) cells, and monocytes (1–4). Alemtuzumab is able to induce a rapid and efficient depletion of T cells from peripheral blood (1–4). Recently, alemtuzumab has been used as an effective induction therapy in solid organ transplants, including kidney, pancreas and intestine (5–8). In transplant recipients, the profound lymphocyte depletion using alemtuzumab shows the potential for excellent graft survival with the development of transplant tolerance (3,9–11).

The mucosal immune system consists of intestinal intraepithelial lymphocytes (IEL) and lamina propria lymphocytes (LPL) resided within highly structured sites. IEL and intestinal epithelial cells are considered to play an important role in the first defense line against microorganisms (12). A large proportion of IEL is composed of TCR$\alpha\beta$- or TCR$\gamma\delta$-positive T cells, which are pivotal in directing and controlling appropriate immunological homeostasis within the gut (13). The gastrointestinal tract is normally colonized with the commensal microbiota. The composition of the commensal microbiota may divergently influence mucosal immune system (14). Recent studies have begun to reveal reciprocal interaction between intestinal immune cells and the gut microbiota (15–19). IELs and LPLs are especially reliant on the commensal microbiota for their proper differentiation and function (15–19). The phenotypic differentiation of specific lymphocyte lineages in the mucosal immune system may be dependent on the distinct component of the microbiota (15,18). The commensal microbiota is actively involved in shaping and maintaining normal mucosal immunity (15,18). Germ-free animals possess an underdeveloped immune system in the gut, and introduction of commensal bacteria induces an expansion of $CD4^+$ T cell and development of organized gut-associated lymphoid tissues (15,17). It has demonstrated a key function of TCR$\gamma\delta^+$ IEL in maintaining host-microbial homeostasis in intestinal inflammation in TCRδ-deficient mice (19). Despite an expanding knowledge on the role of gut microbiota in shaping host immune system, the involvement of mucosal T cell in the colonization of commensal bacteria remains unclear. The profound T cell depletion in peripheral blood could be achieved with alemtuzumab (3,9–11), however, no information is available whether alemtuzumab

induces the depletion of mucosal lymphocyte. Moreover, little is known about the alterations in the intestinal microbiota following mucosal T cell depletion.

In this study, using a cynomolgus monkey model, we aimed to characterize the changes of bacterial community composition after lymphocyte depletion and to define a potential relationship between the commensal microbiota and mucosal lymphocyte. Our data may provide a novel perspective about the relationship between the gut microbiota and host intestinal immune system.

Materials and Methods

Animals

Laboratory-bred cynomolgus monkeys were socially housed at the Laboratory Animal Center, Chinese Academy of Military Medical Sciences (Beijing, China). Fifteen male cynomolgus monkeys (aged 3–5 years, weighing 3.0–5.5 kg) that were verified CD52 antigen negative on erythrocytes, were selected in this study. The selected monkeys were raised in isolated cages with more space to meet their physical and behavioral needs. They were maintained in a room with the temperature set at 20–25°C, humidity ranging from 50% to 75%, and illumination by artificial lighting for 12 h per day. Animal cages and rooms were cleaned and disinfected daily. The monkeys were fed commercially available chow and were allowed *ad libitum* access to clean drinking water. Animals were free of simian immunodeficiency virus SIV), herpes B virus, Bacillus tuberculosis, D-type simian retrovirus, and simian T lymphotrophic virus type 1. All animal procedures and experiments were in accordance with the principles for animal experiments using nonhuman primates (Primate Society of China), and were approved by the laboratory animal care and use committee of Jinling Hospital.

Administration of alemtuzumab and sampling

Cynomolgus monkeys were given the eradication treatment by alemtuzumab regimes as described previously with some modifications (20). Twelve animals were administered intravenously a single dose (3.0 mg/kg, i.v.) of alemtuzumab (MabCampath; Bayer–Schering, Berlin, Germany). After an overnight fast with water *ad libitum*, five biopsy pieces each site (approximately 3 × 3 mm) were taken from the terminal ileum and colon using a paediatric videocolonoscope (Pentax 3440FK, Hamburg, Germany) at 1, 3, 6 or 21 days (three animals each time point) postalumtuzumab infusion for immunofluorescent staining and examination of mucosal microbiota. These animals were euthanatized at 9, 14, 35 or 56 days (three animals each time point) to collect intestinal segments for isolation of IEL and LPL, immunofluorescent analysis and molecular detection of intestinal microbiota. Blood samples were obtained at 1, 3, 6, 9, 14, 21, 35 and 56 days for lymphocyte count and flow cytometric analysis. The remaining three monkeys received a same volume of normal saline but without alemtuzumab administration and were euthanatized to collect the samples of 0 day. Fecal samples were freshly obtained on day 0, 1, 3, 6, 9, 14, 21, 35, 56 and were immediately frozen at –80°C for DNA extraction.

Immunofluorescent staining

The tissue species were embedded in optimum cutting temperature compound (OCT) (Tissue Tek, Sakura, Japan), and were sectioned with a cryostat at 5 μm. After fixation with cold acetone, the cryosections were blocked with 3% bovine serum albumin in phosphate buffered saline (PBS). The sections were incubated with mouse mAb against CD4 or CD8, or rabbit polyclonal antibody to CD45 (Abcam, Cambridge, UK), and were then reacted with secondary antibodies conjugated to Alexa 633 (Molecular Probes, Eugene, OR). Nuclei were counterstained with 4′,6-diamidino-2-phenylindole (DAPI; 1:10,000 dilution; Invitrogen, Life Technologies, Carlsbad, CA, USA). Sections were viewed using a confocal laser scanning microscope (Leica Microsystem, Heidelberg GmbH, Mannheim, Germany). The numbers of positive cells were quantified by NIH Image-Pro Plus 6.0 analyzer software.

Isolation of IEL and LPL

IEL and LPL were isolated as previously described with modification (21,22). In brief, after removing Peyer's patches, the ileal fragments (10 cm) were dissected into short segments (5 mm in length) and stirred in prewarmed Hanks' balanced salt solution (Ca^{2+} and Mg^{2+} free) containing 0.75 mM ethylenediamine tetra acetic acid (EDTA). The tissue slurry was passed through 80- and 400-screen mesh trap valve. The cell suspension was centrifuged to collect cell pellets. The remaining tissues on the trap valve were cut into 1- to 2-mm pieces, and were then shaked in RPMI 1640 medium (GIBCO BRL, Grand Island, NY, USA) containing 15 U/mL collagenase, 100 U/mL penicillin-streptomycin, 25 mM Hepes buffer and 5% fetal calf serum (FCS). LPL cell suspension was obtained as the same procedure above. Discontinuous Percoll density gradient centrifugations were performed to enrich IELs and LPLs. Purified cells were resuspended in RPMI 1640 medium containing 5% FCS and were counted with a hemocytometer. The viability of LPL and IEL was determined by trypan blue exclusion and both were >90%.

Analysis of T cell subsets by flow cytometry

Blood cells, purified IEL and LPL were stained with fluorescein-labeled mAb, including CD3-allophycocyanin (BD Pharmingen, San Diego, CA, USA), CD4-fluorescein isothiocyanate (FITC), CD8-phycoerythrin (PE), CD20-FITC, T-cell receptor (TCR) γδ-PE (eBioscience, San Diego, CA, USA), or TCR αβ-PE (Serotec, Oxford, UK). Blood samples or lymphocyte suspensions (100 μL) were incubated with the antibodies (1:200). Appropriate isotype-matched antibodies were used as negative controls. Cells were run on a FACScan flow cytometer and were analyzed with CellQuest software (BD Bioscience).

DNA extraction and PCR amplification

Mucosa-associated bacterial DNA was extracted using QIAamp DNA Mini Kits (QIAGEN, Valencia, CA, USA) according to the manufacturer's instruction. Community DNA extraction of fecal samples was performed with QIAamp DNA Stool Mini Kits. The extracted DNA was checked by agarose gel electrophoresis (1% w/v) and was quantified spectrophotometrically. The fragments of 16S rRNA gene was amplified by PCR with universal bacterial primers (F357+GC clamp and R518) (23,24). An aliquot of DNA (100 ng) was added into a standard reaction mixture, and PCR reactions were carried out with a touchdown thermocycling program as described previously (24). The amplification products were subjected to electrophoresis in 1% (w/v) agarose gels to identify the purity and correct size.

Denaturing gradient gel electrophoresis

DGGE analysis of PCR amplicons was conducted on a D-Code universal mutation detection system (Bio-Rad, Hercules, CA, USA). Amplicons of 16S rDNA were separated with 8% polyacrylamide gels (acrylamide:bisacrylamide, 37.5:1) containing a linear urea-formamide gradient from 30 to 50%. Electrophoresis was done in 1×TAE buffer (0.8 mM Tris, 0.4 mM acetic acid, 0.8 mM EDTA) at a constant voltage of 120 V at 60°C for 7.5 h. The gels were stained by SYBR Green I (Invitrogen) and photographed by UV transillumination with ChemiDOC™ XRS instrument (Bio-Rad). Scanned images of electrophoretic gels were analyzed using QuantityOne software (Version 4.2, Bio-Rad). The similarities between DGGE profiles were assessed by the Dice coefficient and the unweighted pair group method with the arithmetic average (UPGMA) clustering algorithm, and the corresponding dendrograms were constructed. The relative quantity of a given band was expressed as a fraction (%) of the sum of all defined bands in the same lane (25).

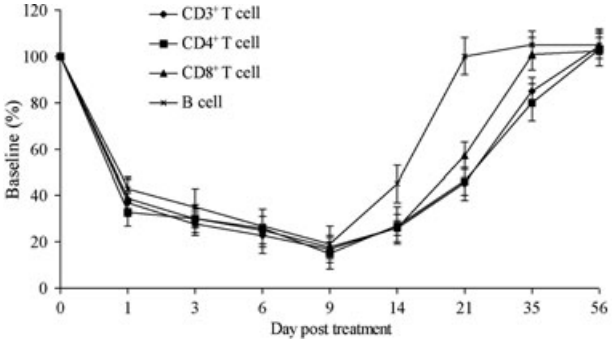

Figure 1: The depletion and repopulation in peripheral blood lymphocytes after the administration of alemtuzumab treatment in cynomolgus monkeys. Results shown here are the mean ± SD of individual animal (n = 3 each time point) and are expressed as the percent (%) of remaining cells after treatment relative to the monkeys of 0 day.

DNA sequencing and phylogenetic analysis

The DGGE bands were excised for determination of DNA sequence. Gel slices were then incubated in 20 μL of elution buffer overnight at 4°C. The resulting DNA solution (4 μL) was used as a template for re-amplification and PCR product was checked by DGGE according to previous procedure (24). The re-amplified fragments were purified and subjected to automated sequence analysis on an ABI PRISM 3730 sequencing system (Applied Biosystems, Foster City, CA, USA). The retrieved sequences were compared in the Genbank database using BLAST algorithm to search for the closest bacterial relatives. Multiple sequence alignments of the nucleotide sequences were performed using CLUSTAL W program. A neighbour-joining tree was generated on the basis of evolutionary distances using MEGA 4.0 software.

Statistical analysis

Data are presented as means ± standard deviation (SD). Statistical analysis was performed by one-way analysis of variance (ANOVA) followed by the Holme–Sidak test using the SPSS software (version 12.0). Correlative analysis between two variances was carried out using linear regression analysis with a Pearson test. A p value of less than 0.05 was considered significant.

Results

Lymphocyte depletion in peripheral blood

The depletion and reconstitution of lymphocytes in peripheral blood was observed following alemtuzumab administration (Figure 1). The numbers of peripheral lymphocytes, including $CD3^+$, $CD4^+$, $CD8^+$ T cells and B cells, reduced to 60% of the baseline levels on day 1 after the infusion (vs. 0 day, $p < 0.01$). Subsequently, a trend towards more depletion of lymphocytes was observed, and the cell counts reached less than 20% at 9 days (vs. 0 day, $p < 0.01$). The initiation of cell repopulation could be found on day 14, and lymphocytes were recovered after 21 days.

Depletion and repopulation of lymphocytes in intestinal mucosa

T-cell depletion in peripheral blood prompted us to test the susceptibility of mucosal lymphocytes to alemtuzumab. $CD4^+$, $CD8^+$ and $CD45^+$ cells in ileal mucosa reduced significantly on days 6 and 9 compared to 0 day ($p < 0.05$; Figures 2A and 2B). The repopulation of mucosal lymphocytes began on day 14, and similar numbers of these cells achieved after 21 days. A similar pattern of lymphocyte depletion and repopulation was noted in the colonal mucosa (Figures 2C and 2D). These results demonstrate that alemtuzumab administration could effectively deplete the lymphocytes in intestinal mucosa.

The shifts of IEL and LPL phenotypes

We further explored the variations of mucosal lymphocyte subsets by flow cytometric analysis. The total numbers of IEL and LPL were lower at 9, 14 and 35 days versus those of 0 day ($p < 0.05$; Figure 3A). Meanwhile, a significant shift in IEL and LPL phenotypes was also observed (Table S1). Significantly lower proportions of $TCR\alpha\beta^+$ and $TCR\gamma\delta^+$ T cells in IELs were measured at 9, 14 and 35 days ($p < 0.01$ or $p < 0.05$, vs. 0 day; Figures 3B and 3C; Table S1). In LPLs, we also found a significant decrease in the proportion of $TCR\gamma\delta^+$ T cells on days 9 and 14 ($p < 0.05$, vs. 0 day). The IEL and LPL subsets were reconstructed after 35 days.

Temporal alterations of ileal mucosa-associated microbiota

We examined whether the structure and composition of the mucosa-associated microbiota was altered in response to lymphocyte depletion (Figure 4A). The dendrogram generated from the DGGE banding patterns showed great variations in the bacterial community after alemtuzumab administration, especially on days 6 and 9 (Figure 4B). Complete linkage hierarchical clustering produced a separated subgroup consisting of the populations of 6 and 9 days**,** with low-community similarities of 54.8% and 49.4% compared to 0 day. The samples taken on days 35 and 56 were assigned into a subcluster, showing increased similarity indices of 78.4% and 82.4% compared to 0 day.

The species richness of intestinal microbiota was evaluated, assessed by the numbers of the DGGE bands. A significant higher richness of ileal mucosal microbiota was observed on days 6, 9 and 14 compared to that of 0 day (30.0 ± 2.1, 28.0 ± 1.7 and 27.0 ± 1.0 vs. 19.7 ± 0.6, $p < 0.01$; Figure 4C). The species richness in the ileal communities of 21 and 35 days reduced back a little bit but was still higher than that of 0 day ($p < 0.01$). Similar numbers of the DGGE bands were restored after 35 days, reflecting the fact that the richness of ileal microbiota was dependent of the lymphocyte residence in the mucosa.

To further investigate the effects of lymphocyte depletion on mucosa-associated flora, we explored the connections between ileal bacterial richness and mucosal lymphocyte. Increased richness in the mucosal microbiota following lymphocyte depletion showed negative correlation with the numbers of IEL and LPL ($r = -0.962$, $p < 0.01$; $r = -0.956$, $p < 0.01$; Figures 4D and 4E). Interestingly, integration of correlations between species richness and $TCR\alpha\beta^+$ or $TCR\gamma\delta^+$ IELs were also determined ($r = -0.941$,

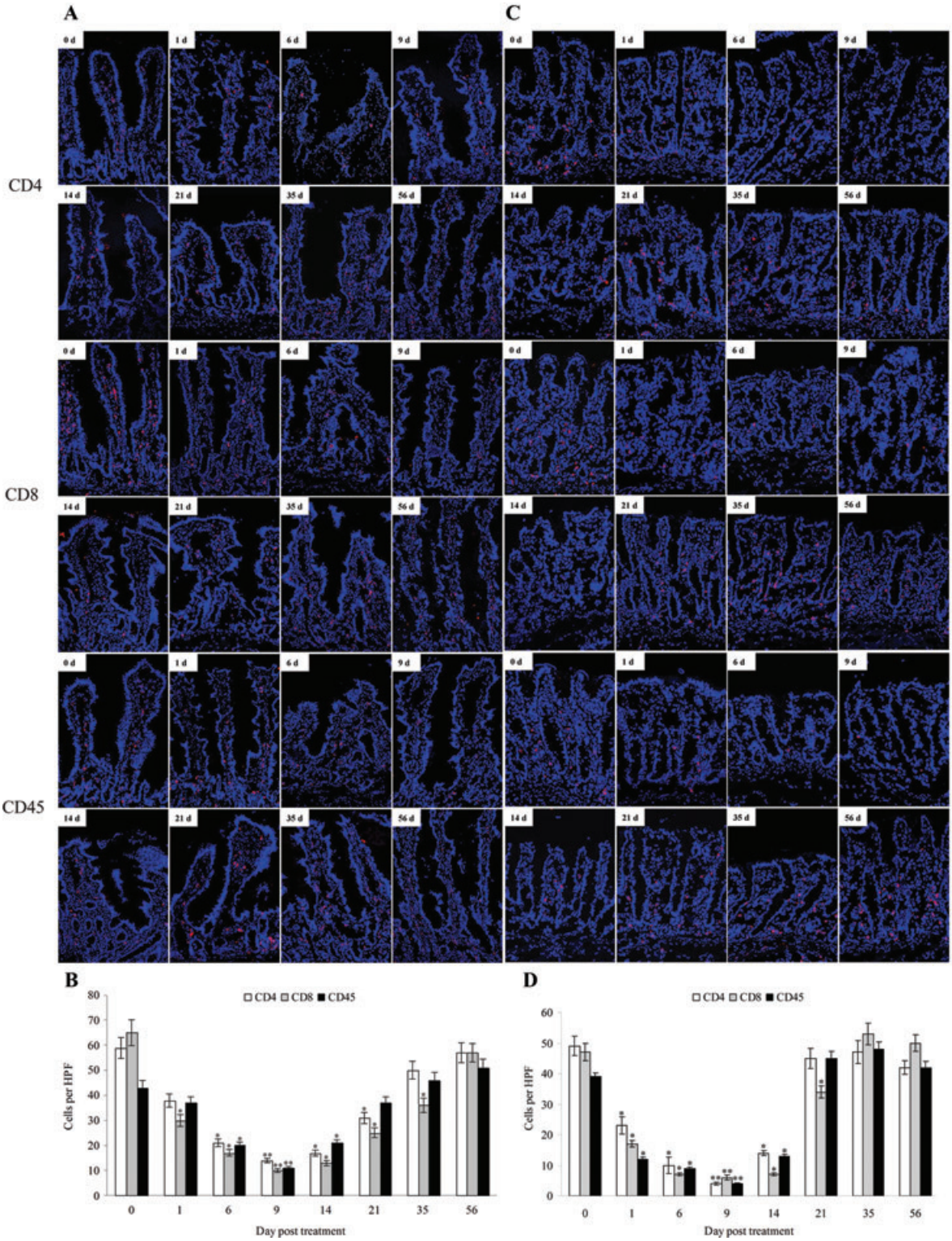

Figure 2: Immunofluorescent analyses of lymphocytes in intestinal mucosa of cynomolgus monkeys by alemtuzumab treatment. Longitudinal visualization of depletion and repopulation of $CD4^+$, $CD8^+$ and $CD45^+$ cells (red) before and after alemtuzumab treatment in the ileum (A) and colon (C) were performed by confocal laser scanning microscopy. Nuclei were counterstained with 4′,6-diamidino-2-phenylindole (DAPI) (blue). The numbers of $CD4^+$, $CD8^+$, and $CD45^+$ cells per HPF (magnification, ×200) in the ileum (B) and colon (D) were measured by Image-Pro Plus 6.0. Data are presented as mean ± SD. *$p < 0.05$, **$p < 0.01$, compared with 0 day.

doi: 10.1111/ajt.12148

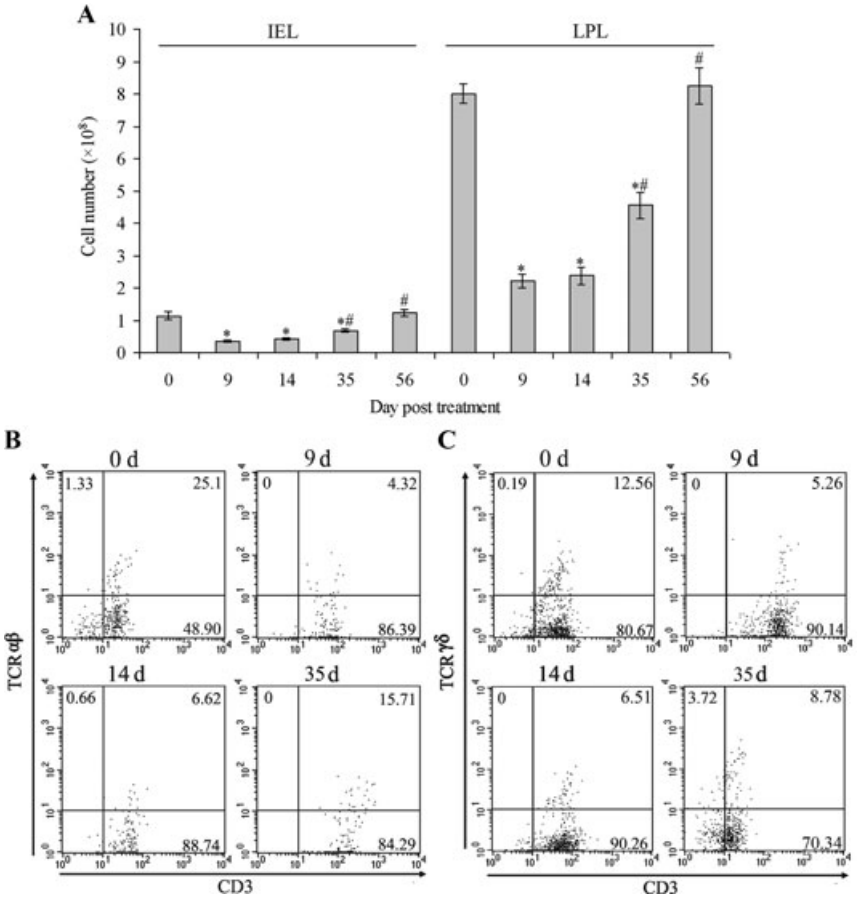

Figure 3: Depletion and repopulation of lymphocytes in intestinal tissues after the administration of alemtuzumab in cynomolgus monkeys. (A) IELs and LPLs were isolated from the ileum tissues, which were collected at indicated time points, and their numbers were counted with a hemocytometer. Data are presented as mean ± SD. *$p < 0.05$, compared with 0 day; #$p < 0.05$, compared with 9 days. Representative histograms of flow cytometry showing dynamics of percentage of $CD3^+TCR\alpha\beta^+$ IELs (B) and $CD3^+TCR\gamma\delta^+$ IELs (C).

$p < 0.01$; $r = –0.927$, $p < 0.01$, respectively; Figures 4F and 4G). The results provide a clear demonstration that the perturbation of the microbiota composition in ileal mucosa is associated with lymphocyte depletion.

Alterations of predominant bacterial species in ileal mucosa

To characterize the bacterial lineages presented in the ileal mucosa after T cell depletion, we performed sequencing analysis for identification of the predominant microbial phylotypes. The bacterial species retrieved from the BLAST algorithm were mostly belonged to three populated bacterial taxa, namely the orders Lactobacillales and Enterobacteriales, and the genus Prevotella (Figure 4H). The members of the Lactobacillales order, such as *Lactobacillus capillatus* (I1), *Lactococcus plantarum* (I5) and *Weissella cibaria* (I2), composed on average 60% of the predominant bacteria in animals of 0 day, whereas the proportion declined to 49% and 40% at 6 and 9 days ($p < 0.05$; Figure 4I, Table S2). A higher concentration of the Prevotella bacteria that was absent in the animals of 0 day, including *Prevotella copri* (I3) and *Prevotella dentalis* (I12), was detected in the mucosa-associated microbiota at 6, 9 and 14 days (21%, 22% and 14% vs. 0 day, $p < 0.01$). The bacterial species of the Enterobacteriales order, *Escherichia coli* (I14) and *Shigella flexneri* (I13), were more presented on day 9 than that of 0 day (18% vs. 6%, $p < 0.01$). Strikingly, the occurrences of the bacterial taxa were nearly normalized after 35 days. The differential distribution of the bacterial phylotypes over time delineates unique effects of lymphocytes depletion on the microbiota composition.

Altered bacterial community composition in colonal mucosa

The response of colonal mucosa-associated microbiota to lymphocyte depletion was then evaluated (Figure 5A). Lymphocyte depletion induced a significant perturbation of microbiota composition, resulting in low-similarity profiles ranging from 45.5% to 58.4% between 0 day and the samples obtained from 1 to 14 days (Figure 5B). Following the reconstitution of lymphocytes, the colonal mucosal populations showed a tendency towards normalized pattern of bacterial distributions. Compared to 0 day, the community structure at 35 and 56 days had a similarity coefficient of 72.3% and 78.1%, respectively.

As expected, lymphocyte depletion resulted in a dramatic shift of the predominantly bacterial phylotypes in colonal mucosa. The phylogenetic plot of the bacteria identified in the colonal mucosa showed that the majority of the

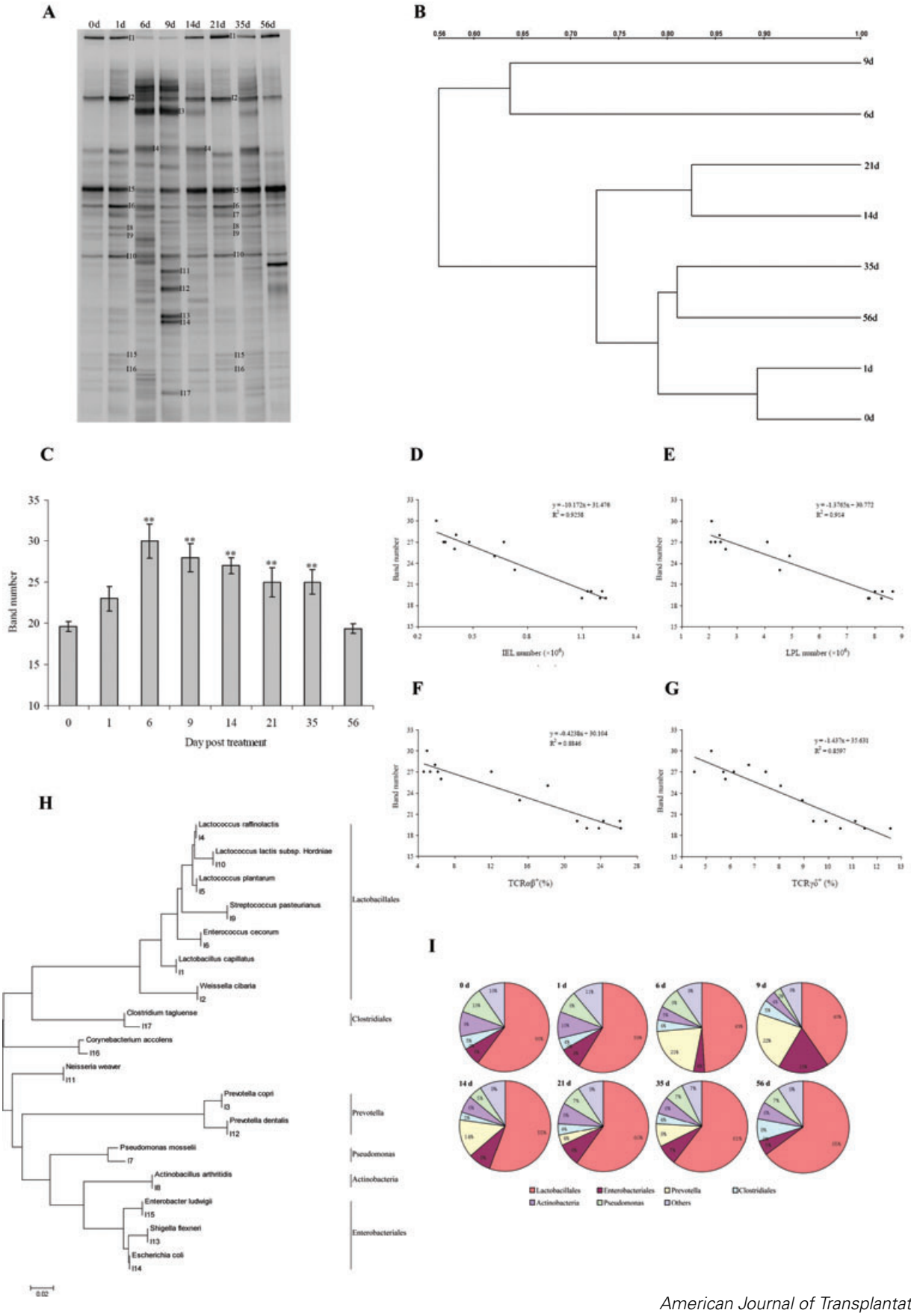
A
0d 1d 6d 9d 14d 21d 35d 56d
B
9d
6d
21d
14d
35d
56d
1d
0d
C
Band number
Day post treatment
D
E
F
G
H
Lactococcus raffinolactis
Lactococcus lactis subsp. Hordniae
Lactococcus plantarum
Streptococcus pasteurianus
Enterococcus cecorum
Lactobacillus capillatus
Weissella cibaria
Clostridium tagluense
Corynebacterium accolens
Neisseria weaver
Prevotella copri
Prevotella dentalis
Pseudomonas mosselii
Actinobacillus arthritidis
Enterobacter ludwigii
Shigella flexneri
Escherichia coli
Lactobacillales
Clostridiales
Prevotella
Pseudomonas
Actinobacteria
Enterobacteriales
I
Lactobacillales
Enterobacteriales
Prevotella
Clostridiales
Actinobacteria
Pseudomonas
Others

microbial population was associated with three bacterial taxa: the orders Lactobacillales and Enterobacteriales and the Bacteroides genus (Figure 5C). The enteric cocci from the Lactobacillales order, especially *Streptococcus caballi* (C7) and *Enterococcus columbae* (C8) and *Streptococcus pasteurianus* (C10), were overrepresented in the mucosal microbiota on days 1 and 6 (47% and 31% vs. 18% of 0 day, $p < 0.01$; Figure 5D; Table S3). The bacterial populations of the Bacteroides genus, *Bacteroides intestinalis* (C4) and *Bacteroides nordii* (C4), reduced at 1 and 6 days, accounting for only 10% and 9% of the enrichment (vs. 23% of 0 day, $p < 0.01$). Additionally, an increased proportion in the Enterobacteriales order was measured in the colonal mucosa after the infusion ($p < 0.01$). It was noteworthy that the predominantly bacterial composition was recovered following the reconstitution of lymphocytes.

Variations of the dominant fecal microbiota

We next assessed whether the structure and composition of the fecal microbiota were affected by lymphocyte depletion (Figure 6A). A significant variation in fecal community structure were resulted from the lymphocyte depletion, as characterized by low similarity ranging from 43.4% to 57.1% in 21-day duration of alemtuzumab treatment compared with 0 day (Figure 6B). It suggested that fecal microbial composition was altered pronouncedly following the depletion of lymphocytes. The overall phylogenetic distribution of the bacterial species obtained from the faeces was shown in Figure 6C. In comparison to 0 day, the members of the Clostridiales order were more abundant on days 1, 3, 6 and 9, whereas *Faecalibacterium prausnitzii* less abundant on days 3, 6, 9, 14 and 21 (Figure 6D; Table S4). The proportions of the predominantly bacterial subgroups went back to normalized after 35 days.

Discussion

The human gut is the primary site of the interaction between commensal microbiota and mucosal immune system. It has been established that gut bacteria are crucial for the development and function of the intestinal immune system (15,18). The distinct component of the gut microbiota could play a role in the differentiation of certain T cell subsets (26). Dysbiosis of the microbiota could reprogram intestinal immune responses (27), however, how the intestinal immune cells, specifically IEL and LPL, affect the microbiota composition in the intestinal mucosa, is still unknown. In this study, we characterize the bacterial community composition after lymphocyte depletion. We demonstrate that intestinal microbiota is perturbed after mucosal T cells are depleted, and it is subsequently restored following the reconstruction of the lymphocytes. We also document large compositional shifts in the specific bacterial taxa including Lactobacillales, Enterobacteriales, Clostridiales, Prevotella and Faecalibacterium over time of T cell depletion. More importantly, mucosal lymphocytes, especially TCR$\alpha\beta^+$ and TCR$\gamma\delta^+$ T cells, are associated with species richness of mucosa-associated microbiota. Our findings demonstrate the importance of mucosal T cell in maintaining the homeostasis of the gut microbiota and further emphasize reciprocal interaction between the host immune system and commensal microbiota.

Alemtuzumab is a humanized monoclonal antibody engineered with a human fragment crystalizable (Fc) region, and it could specifically recognize human CD52 antigen and induces a profound depletion of lymphocytes and monocytes (1–4,28). The macaque species are phylogenetically proximate to human and alemtuzumab crossreacts with macaques (20,29). Alemtuzumab is not equivalently recognized by murine or rat effector cells (20). Nonhuman primates are the most informative animal models for alemtuzumab in transplantation research (29–31). Since the antibody also recognizes CD52-positive erythrocytes in nonhuman primates, it is important that the cynomolgus monkey could be selected for CD52 antigen negative on erythrocytes (20). In this study, cynomolgus monkeys with CD52 antigen negative on erythrocytes are selected for the experiment.

The roles of gut microbiota in the development of immune system have been well known, however, it remains speculative whether mucosal lymphocytes influence the indigenous commensal microflora. The results presented here show that the gut microbiota is substantially perturbed by the depletion of intestinal lymphocyte (Figures 4A, 5A and 6A). The commensal microbiota subsequently began to recover from the perturbation and to reach normal state following lymphocyte repopulation. The findings support the concept that mucosal lymphocyte plays a critical role in maintaining the balance of the commensal microbiota.

The intestinal microbiota composition, especially important candidate bacterial species, may be influenced by mucosal lymphocyte depletion. In the analysis of the major bacterial taxa, we show that microbial population composition, in particular the bacteria from Lactobacillales,

◀ **Figure 4: Alterations of the composition of ileal mucosa-associated microbiota with the administration of alemtuzumab. (A) Representative DGGE plots of ileal microbiota.** I1 to I17 represent the prodominant bands. (B) Dendrogram of community similarities drawn from DGGE fingerprints. The dendrogram was constructed using the unweighted pair group method with arithmetic means (UPGMA), and the scale bar indicates similarity (%). (C) Comparison of bacterial diversity. Results are expressed as band numbers and values are shown as mean ± SD ($n = 3$ each time point). *$p < 0.05$, **$p < 0.01$, compared with 0 day. Correlative analysis between band numbers and the numbers of IEL (D) or LPL (E), the proportions of TCR$\alpha\beta^+$ (F) or TCR$\gamma\delta^+$ cells (G). (H) Phylogenetic tree of sequences of the identified bands in the gel and their nearest neighbors form the NCBI GenBank databases, using the neighbor-joining method by MEGA 4.0. (I) Aggregate of microbiota composition by relative intensity of sequenced DNA bands after alemtuzumab treatment.

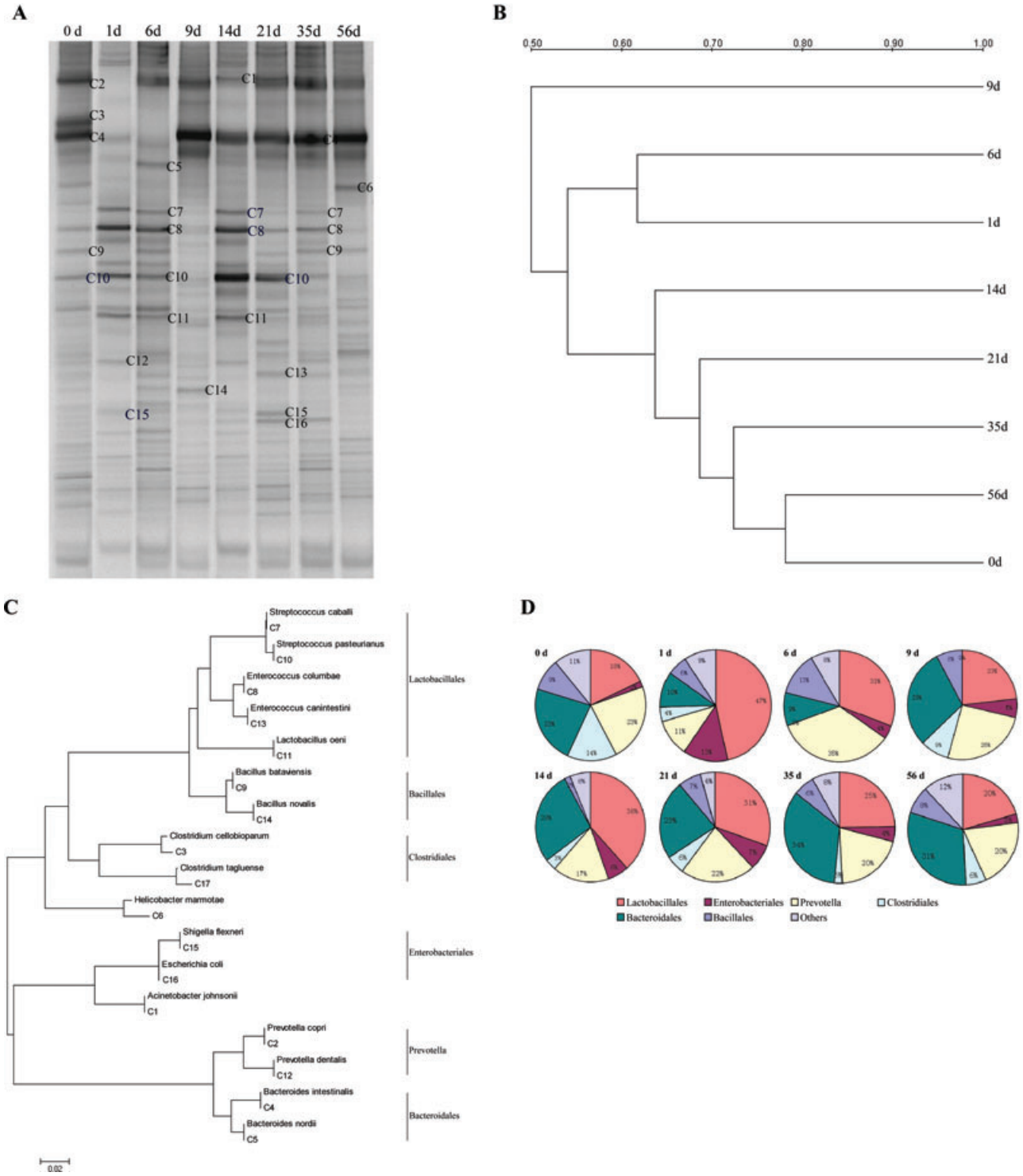

Figure 5: Shifts of colonal microbiota composition in the depletion and repopulation of lymphocytes. (A) Representative DGGE profiles of colonal microbiota at different time points post alemtuzumab treatment. C1 to C17 indicate the prominent bands for DNA sequencing. (B) Dendrogram of community similarities drawn from DGGE fingerprints. (C) Phylogenetic tree generated from the 16S rDNA sequences of predominant bacterial species in the conon (D) Analysis of the relative quantity in the sequenced DNA bands.

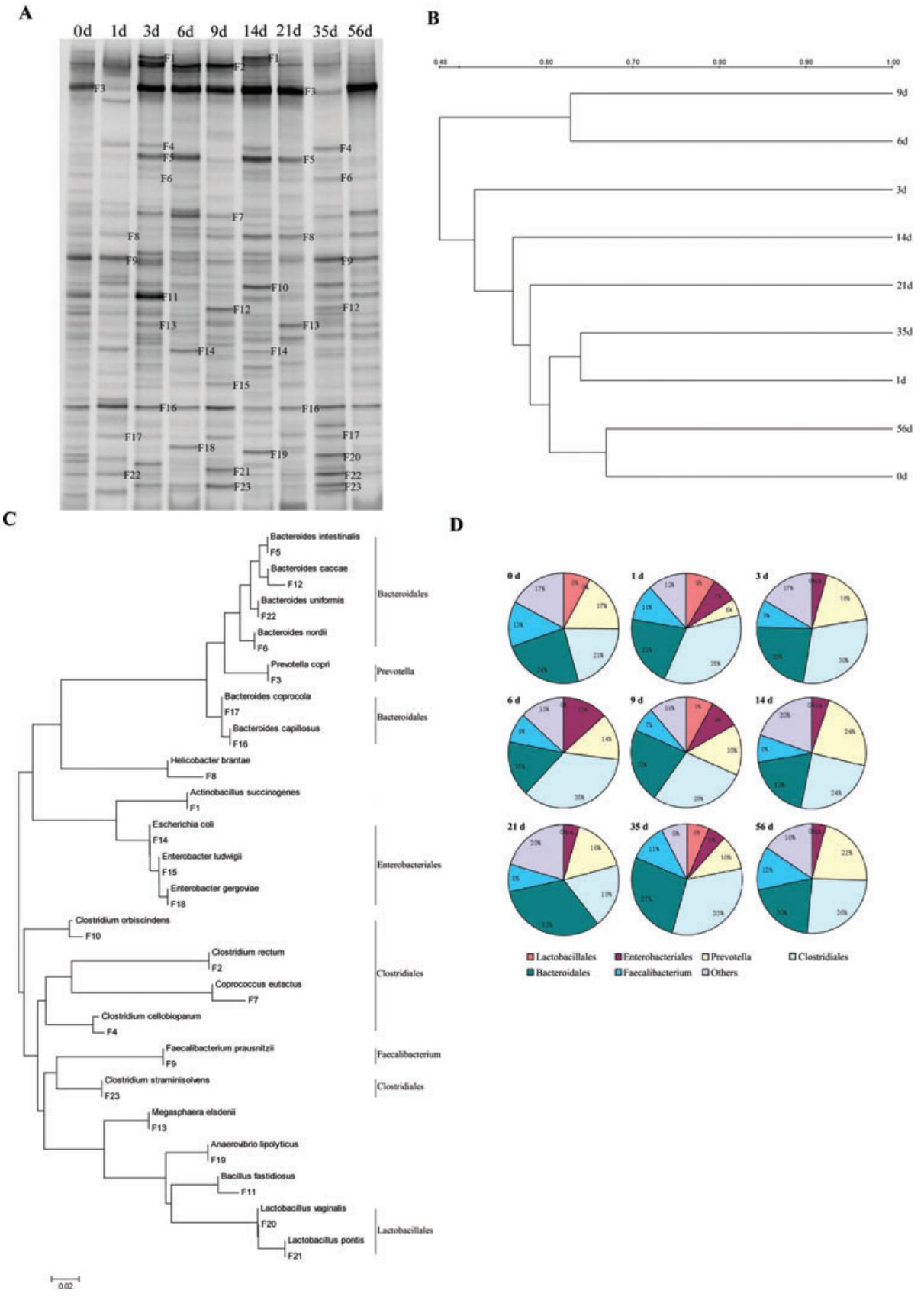
A
0d 1d 3d 6d 9d 14d 21d 35d 56d
B
0.40 0.60 0.70 0.80 0.90 1.00
9d
6d
3d
14d
21d
35d
1d
56d
0d
C
Bacteroides intestinalis F5
Bacteroides caccae F12
Bacteroides uniformis F22
Bacteroides nordii F6
Prevotella copri F3
Bacteroides coprocola F17
Bacteroides capillosus F16
Helicobacter brantae F8
Actinobacillus succinogenes F1
Escherichia coli F14
Enterobacter ludwigii F15
Enterobacter gergoviae F18
Clostridium orbiscindens F10
Clostridium rectum F2
Coprococcus eutactus F7
Clostridium cellobioparum F4
Faecalibacterium prausnitzii F9
Clostridium straminisolvens F23
Megasphaera elsdenii F13
Anaerovibrio lipolyticus F19
Bacillus fastidiosus F11
Lactobacillus vaginalis F20
Lactobacillus pontis F21
Bacteroidales
Prevotella
Bacteroidales
Enterobacteriales
Clostridiales
Faecalibacterium
Clostridiales
Lactobacillales
0.02
D
0 d
1 d
3 d
6 d
9 d
14 d
21 d
35 d
56 d
Lactobacillales
Enterobacteriales
Prevotella
Clostridiales
Bacteroidales
Faecalibacterium
Others

Enterobacteriales and Prevotella, is strongly altered with the depletion of mucosal T cells. The specific members of the Lactobacillales order, including *Lactobacillus* spp. and *Weissella cibaria*, is dominated in the ileal mucosa prior alemtuzumab adminastration, while their abundance is strikingly reduced after the depletion of mucosal T cells. Components of the Lactobacillales order are mostly characterized as the commensal organisms and are beneficial in nature for the maintenance of normal microbiota structure (32–34). Reduced colonization in these bacterial species in ileal mucosa is probably an important signature of mucosa-associated microbiota dysbiosis. In addition, it is interesting that the members of the Enterobacteriales order show an increase in the proportions after mucosal lymphocyte depletion. The bacterial species of the Enterobacteriales order, such as *Escherichia coli*, *Shigella flexneri* and *Enterobacter ludwigii*, are considered as opportunistic organisms and are less colonized in intestinal mucosa (35–37). An increase in adherent *Escherichia coli* in intestinal mucosa is associated with chronic intestinal inflammation (35,36). Another noteworthy observation is that the Prevotella bacteria are present exclusively in ileal mucosa after the depletion of intestinal lymphocytes, suggesting that the Prevotella genus might be susceptible to the loss of mucosal lymphocyte. The Prevotella bacteria adhered in the mucosa is able to digest mucins and it may lead to the impairment of mucosal architecture (38). The proportions of these bacteria, including the taxa Lactobacillales, Enterobacteriales and Prevotella, are recovered with the reconstruction of mucosal T cells. We further investigate the shifts in predominant bacterial species in the colon during the depletion and repopulation of mucosal lymphocytes. The altered proportions in the Lactobacillales and Bacteroides orders are mainly observed in colonal mucosa in response to lymphocyte depletion (Figure 5D). An increased colonization by Lactobacillales, especially *Streptococcus* spp. and *Enterococcus columbae*, while a less abundance in the Bacteroides order, are seen in colonal mucosa following lymphocyte depletion. The Bacteroides is normally resided in the colon mucosa and plays a crucial role in maintaining the homeostasis of mucosal immune system (39). Taken together, our findings suggest that the commensal microbiota are in response to T cell depletion and the shifts of specific bacterial species might be associated with the lymphocyte depletion.

The impact of intestinal T cell subsets on microbial colonization remains largely unexplored. We show that the proportions of TCR$\alpha\beta^+$ and TCR$\gamma\,\delta^+$ IELs are reduced, indicating an imbalance of T cell phenotypes in intestinal mucosa after lymphocyte depletion (Figures 3B, 3C). Importantly, the percentages of TCR$\alpha\beta^+$ and TCR$\gamma\,\delta^+$ cells in IELs are correlated with the alterations in bacterial diversity (Figures 4F and 4G). The microbial colonization can induce a dramatic expansion of TCR$\alpha\beta^+$ T cells in germ-free mice (40). TCR$\gamma\,\delta^+$ T cells are essential for controlling mucosal penetration of commensal bacteria in intestinal inflammation, implying a key function of TCR$\gamma\,\delta^+$ IEL in acute mucosal injury (19). TCR$\gamma\,\delta^+$ IELs provide essential antibacterial protection of the mucosal surface and could be critical mediators of homeostasis between humans and their microbiota (41). Our results indicate that TCR$\alpha\beta^+$ and TCR$\gamma\,\delta^+$ IEL are associated with the alterations of microbial composition after lymphocyte depletion, which provides novel evidence for the reciprocal interaction between T cell subsets and the commensal microbiota.

In summary, this study is the first description for the characteristic of gut microbiota changes in response to lymphocyte depletion. Differential distributions of specific bacterial phylotypes, in particular the orders of Lactobacillales, Enterobacteriales and Clostridiales, and the genus of Prevotella and Faecalibacterium, are primarily to define the dysbiosis of the microbiota following lymphocyte depletion. We demonstrate an association between the perturbation of gut microbiota and lymphocyte depletion, indicating the dominant role of mucosal lymphocytes in shaping the microbial composition of the gut. Elucidation of the relationship between the gut microbiota and mucosal immune system would provide new information to the effect of alemtuzumab on immune tolerance induction in organ transplantation.

Acknowledgments

The authors thank the Deutscher Akademischer Austauschdienst Researcher Fellowship (Bioscience Special Program, Germany) for Dr. Qiurong Li.

Funding source:

This work was supported by the National Basic Research Program (973 Program) in China (2013CB531403 and 2009CB522405), National High-tech R&D Program (863 Program) of China (2012AA021007), National Natural Science Foundation in China (81070375) and Scientific Research Fund in Jiangsu Province (BK2009317).

Disclosure

The authors of this manuscript have no conflicts of interest to disclose as described by the *American Journal of Transplantation*.

◀ **Figure 6: Molecular analysis of fecal microbiota after administration with alemtuzumab.** (A) Representative fingerprints of DGGE gels for the fecal microbiota. F1 to F23 represent most prominent bands. (B) Dendrogram of community similarities drawn from DGGE profiles. The scale bar indicates similarity (%). (C) Phylogenetic relationship of 16S rDNA sequences obtained from the fecal specimens. (D) Variations of relative proportions in the aggregate microbiota after alemtuzumab treatment.

References

1. Hale G, Dyer MJ, Clark MR, et al. Remission induction in non-Hodgkin lymphoma with reshaped human monoclonal antibody CAMPATH-1H. Lancet 1988; 2: 1394–1399.
2. Flynn JM, Byrd JC. Campath-1H monoclonal antibody therapy. Curr Opin Oncol 2000; 12: 574–581.
3. Ciancio G, Burke GW, Gaynor JJ, et al. A randomized trial of thymoglobulin vs. alemtuzumab (with lower dose maintenance immunosuppression) vs. daclizumab in renal transplantation at 24 months of follow-up. Clin Transplant 2008; 22: 200–210.
4. Margreiter R, Klempnauer J, Neuhaus P, et al. Alemtuzumab (Campath-1H) and tacrolimus monotherapy after renal transplantation: Results of a prospective randomized trial. Am J Transplant 2008; 8: 1480–1485.
5. Calne R, Moffatt SD, Friend PJ, et al. Prope tolerance with induction using campath 1H and low-dose cyclosporin monotherapy in 31 cadaveric renal allograft recipients. Nippon Geka Gakkai Zasshi 2000; 101: 301–306.
6. Knechtle SJ, Pirsch JD, Fechner H, et al. Campath-1H induction plus rapamycin monotherapy for renal transplantation: Results of a pilot study. Am J Transplant 2003; 3: 722–730.
7. Garcia M, Weppler D, Mittal N, et al. Campath-1H immunosuppressive therapy reduces incidence and intensity of acute rejection in intestinal and multivisceral transplantation. Transplant Proc 2004; 36: 323–324.
8. Kandaswamy R, Gruessner R, Gruessner A, et al. Calcineruin inhibitor (CI) and steroid-free immunosuppression (ImmSx) for pancreas (Px) and px-kidney (KD) recipients using campath for both induction and maintenance (Maint.). Am J Transplant 2004; 4: 536.
9. Pascual J, Bloom D, Torrealba J, et al. Calcineurin inhibitor withdrawal after renal transplantation with alemtuzumab: Clinical outcomes and effect on T-regulatory cells. Am J Transplant 2008; 8: 1529–1536.
10. Tan HP, Donaldson J, Basu A, et al. Two hundred living donor kidney transplantations under alemtuzumab induction and tacrolimus monotherapy: 3-year follow-up. Am J Transplant 2009; 9: 355–366.
11. Newell KA, Cendales LC, Kirk AD. Finding the right job for the tool: Alemtuzumab and its role in renal transplantation. Am J Transplant 2008; 8: 1363–1364.
12. Pitman RS, Blumberg RS. First line of defense: The role of the intestinal epithelium as an active component of the mucosal immune system. J Gastroenterol 2000; 35: 805–814.
13. Beagley KW, Husband AJ. Intraepithelial lymphocytes: Origins, distribution, and function. Crit Rev Immunol 1998; 18: 237–254.
14. Fujiwar D, Wei B, Presley LL, et al. Systemic control of plasmacytoid dendritic cells by $CD8^+$ T cells and commensal microbiota. J Immunol 2008; 180: 5843–5852.
15. Macpherson AJ, Harris NL. Interactions between commensal intestinal bacteria and the immune system. Nature Rev Immunol 2004; 4: 478–485.
16. Bäckhed F, Ley RE, Sonnenburg JL, et al. Host-bacterial mutualism in the human intestine. Science 2005; 307: 1915–1920.
17. Duan JY, Kasper DL. Regulation of T cells by gut commensal microbiota. Curr Opin Rheumatol 2011; 23: 372–376.
18. Round JL, Mazmanian SK. The gut microbiota shapes intestinal immune responses during health and disease. Nat Rev Immunol 2009; 9: 313–323.
19. Ismail AS, Behrendt CL, Hooper LV. Reciprocal interactions between commensal bacteria and $\gamma\delta$ intraepithelial lymphocytes during mucosal injury. J Immunol 2009; 182: 3047–3054.
20. van der Windt DJ, Smetanka C, Macedo C, et al. Investigation of lymphocyte depletion and repopulation using alemtuzumab (Campath-1H) in cynomolgus monkeys. Am J Transplant 2010; 10: 773–783.
21. Guy-Grand D, Griscelli C, Vassali P. The mouse gut T lymphocyte, a novel type of T cell: Nature, origin and traffic in mice in normal and graft versus-host conditions. J Exp Med 1978; 148: 1661.
22. Lefrancois L. Carbohydrate differentiation antigens of murine T cells: Expression on intestinal lymphocytes and intestinal epithelium. J Immunol 1987; 138: 3375–3384.
23. Vanhoutte T, Preter VD, Brandt ED, et al. Molecular monitoring of the fecal microbiota of healthy human subjects during administration of Lactulose and Saccharomyces boulardii. Appl Environ Microbiol 2006; 72: 5990–5997.
24. Li Q, Zhang Q, Wang C, et al. Fish oil enhances recovery of intestinal microbiota and epithelial integrity in chronic rejection of intestinal transplant. PLoSONE 2011; 6: e20460.
25. Bercik P, Denou E, Collins J, et al. The intestinal microbiota affect central levels of brain-derived neurotropic factor and behavior in mice. Gastroenterology 2011; 141: 599–609.
26. Smith PM, Garrett WS. The gut microbiota and mucosal T cells. Front Microbiol 2011; 2: 1–6.
27. Leea YK, Menezesa JS, Umesakib Y, et al. Proinflammatory T-cell responses to gut microbiota promote experimental autoimmune encephalomyelitis. Proc Natl Acad Sci USA 2011; 108: 4615–4622.
28. Hale G. CD52 (CAMPATH1). J Biol Regul Homeost Agents 2002; 15: 386–391.
29. Knechtle SJ, Burlingham WJ. Metastable tolerance in nonhuman primates and humans. Transplantation 2004; 77: 936–939.
30. Cendales LC, Xu H, Bacher J, et al. Composite tissue allotransplantation: Development of a preclinical model in nonhuman primates. Transplantation 2005; 80: 1447–1454.
31. Tseng YL, Sachs DH, Cooper DK. Porcine hematopoietic progenitor cell transplantation in nonhuman primates: A review of progress. Transplantation 2005; 79: 1–9.
32. Bibiloni R. VSL#3 probiotic-mixture induces remission in patients with active ulcerative colitis. Am J Gastroenterol 2005; 100: 1539–1546.
33. Reid G. The scientific basis for probiotic strains of Lactobacillus. Appl Environ Microbiol 1999; 65: 3763–3766.
34. Vaughan EE, Mollet B, deVos WM. Functionality of probiotics and intestinal lactobacilli: Light in the intestinal tract tunnel. Curr Opin Biotechnol 1999; 58: 505–510.
35. Darfeuille-Michaud A, Boudeau J, Bulois P, et al. High prevalence of adherent-invasive *Escherichia coli* associated with ileal mucosa in Crohn's disease. Gastroenterology 2004; 127: 412–421.
36. Martin HM, Campbell BJ, Hart CA, et al. Enhanced *Escherichia coli* adherence and invasion in Crohn's disease and colon cancer. Gastroenterology 2004; 127: 80–93.
37. Swidsinski A, Ladhoff A, Pernthaler A et al. Mucosal flora in inflammatory bowel disease. Gastroenterology 2002; 122: 44–54.
38. Rausch P, Rehman A,Künzel S, et al.Colonic mucosa-associated microbiota is influenced by an interaction of Crohn disease and FUT2 (Secretor) genotype. Proc Natl Acad Sci USA 2011; 108: 19030–19035.
39. Kelly D, Campbell JI, King TP, et al. Commensal anaerobic gut bacteria attenuate inflammation by regulating nuclear-cytoplasmic shuttling of PPAR-gamma and RelA. Nat Immunol 2004; 5: 104–112.
40. Umesaki Y, Setoyama H, Matsumoto S et al. Expansion of $\alpha\beta^+$ T-cell receptor-bearing intestinal intraepithelial lymphocytes after

microbial colonization in germ-free mice and its independence from thymus. Immunology 1993; 79: 32–37.
41. Ismail AS,.Severson KM, Vaishnava S, et al. γδ intraepithelial lymphocytes are essential mediators of host–microbial homeostasis at the intestinal mucosal surface. Proc Natl Acad Sci USA 2011; 108: 8743–8748.

Supporting Information

Additional Supporting Information may be found in the online version of this article at the publisher's website:

Table S1: The phenotypes in intestinal intraepithelial lymphocytes and lamina propria lymphocytes

Table S2: The sequence analysis of DGGE bands from the ileal mucosa

Table S3: The sequence analysis of DGGE bands from colonal mucosal samples

Table S4: The sequence analysis of DGGE bands from the fecal specimens